Active site assembly by SMG5 as a mechanism for SMG6 endonuclease licensing in nonsense-mediated mRNA decay

Enes S. Arpa[1*], Michael Taschner[2*], Mara De Matos[1], Stefanie Jonas[3#], David Gatfield[1#]

Affiliations:

[1] Center for Integrative Genomics (CIG), University of Lausanne, 1015 Lausanne, Switzerland.

[2] Department of Fundamental Microbiology (DMF), University of Lausanne, 1015 Lausanne, Switzerland.

[3] Department of Biology, Institute of Molecular Biology and Biophysics, ETH Zurich, 8093 Zurich, Switzerland.

[*] shared first authorship

[#] corresponding authors

e-mail addresses: enessalih.arpa@unil.ch, michael.taschner@unil.ch, mara.dematos@unil.ch, stefanie.jonas@mol.biol.ethz.ch, david.gatfield@unil.ch

Abstract

Nonsense-mediated mRNA decay (NMD) is a conserved eukaryotic surveillance pathway that eliminates transcripts containing premature termination codons (PTCs). While the recognition phase of NMD is well characterised, the effector step – how targeted mRNAs are nucleolytically degraded – remains incompletely understood. In metazoans, NMD employs an endonucleolytic route mediated by SMG6, a PIN-domain nuclease, alongside SMG5 and SMG7, which act downstream of PTC recognition. SMG5 has recently been proposed to license SMG6 activity, yet the molecular basis of this licensing has remained elusive. Here, we combine AlphaFold structural predictions with biochemical assays to investigate interactions among human SMG5, SMG6, and SMG7. Structural models predict a high-confidence interface between SMG5 and SMG6 PIN domains that forms a composite active site: a conserved SMG5 aspartate (D893) complements the SMG6 acidic triad to create the canonical quartet required for PIN nuclease activity. *In vitro*, SMG6 alone exhibits weak endonucleolytic activity, which is enhanced ~10-fold by SMG5 PIN. Mutational analyses confirm that conserved residues from both proteins are essential for this composite configuration. Our findings reveal that the SMG5 PIN domain, previously considered catalytically inert, plays a critical role in activating SMG6 by completing its active site. This work provides mechanistic insight into the SMG5-dependent licensing step and uncovers a composite PIN nuclease architecture at the heart of the metazoan NMD effector phase.

Keywords: nonsense-mediated mRNA decay (NMD); PIN domain; UPF1 phosphorylation; endonucleolytic decay; SMG5-SMG6 interaction; RNA surveillance; in vitro nuclease assay

Introduction

Nonsense-mediated mRNA decay (NMD) was first recognized more than three decades ago as a conserved eukaryotic mRNA surveillance pathway that selectively degrades transcripts containing premature termination codons (PTCs) [1]. Early genetic screens in *Saccharomyces cerevisiae* [2] and *Caenorhabditis elegans* [3] identified the core Upf (up-frameshift) and Smg (suppressor of morphogenesis on genitalia) factors, defining a pathway that is conserved from yeast to humans. Subsequent work across species has established the “rules of NMD” – i.e., the molecular features that determine whether a terminating ribosome triggers or escapes NMD recognition and activation. By contrast, the effector phase – how targeted transcripts are ultimately degraded – took longer to resolve. NMD was long thought to rely primarily on accelerated general exonucleolytic mRNA turnover rather than specialized nucleases [4, 5]. It is now clear, however, that NMD recruits both exonucleolytic and endonucleolytic decay mechanisms, with striking mechanistic divergence between yeast and metazoans [6].

In yeast, NMD relies predominantly on the canonical decapping-dependent 5'→3' exonucleolytic decay pathway [7]. Once marked for NMD, transcripts are decapped by Dcp1/Dcp2 and rapidly degraded by the 5'→3' exonuclease Xrn1, with the 3'→5' exosome contributing to a lesser extent [4, 8]. This paradigm established NMD as a pathway that co-opts general mRNA decay machinery rather than deploying pathway-specific nucleases.

By contrast, the situation in metazoans is more complex. Two key discoveries reshaped current models: first, that NMD substrates in *Drosophila melanogaster* undergo endonucleolytic cleavage near the PTC [9], and second, that *Drosophila* and human SMG6 proteins harbour an active PIN (PilT N-terminal) endonuclease domain domain [10-12]. In the prevailing model, SMG6 – representing the first dedicated nuclease intrinsic to the NMD machinery – directly cleaves target mRNAs, generating unprotected 3' and 5' fragments that are subsequently cleared by XRN1 and the exosome.

In addition to SMG6, metazoan NMD employs SMG5 and SMG7, factors not found in *S. cerevisiae*. All three proteins act downstream of PTC recognition i.e. after deposition of the central NMD effector helicase UPF1 on the target mRNA has been triggered. They directly associate with different sections

63 of UPF1 [13], with SMG6 engaging the UPF1 N-terminus, the helicase domain [14] and a helicase
64 regulating domain [15], while the SMG5-SMG7 module recognises C-terminal (phospho-)residues
65 [16]. Historically, SMG5-SMG7 was viewed primarily as a heterodimeric adaptor that recruits general
66 mRNA turnover enzymes – including the CCR4–NOT deadenylase complex and decapping factors
67 [17-19] – thereby providing an exonucleolytic route analogous to the yeast mechanism. Although
68 early work suggested that SMG6-mediated endo-cleavage and SMG5-SMG7-mediated
69 exonucleolytic decay act in parallel and redundantly on overlapping sets of transcripts [20], more
70 recent evidence supports a linear pathway, in which SMG5-SMG7 function upstream of SMG6
71 activation [21-23]. In particular, SMG5 has been proposed to act as a licencing factor for SMG6, such
72 that SMG6 is recruited to UPF1 but requires a SMG5-SMG7-dependent authorisation step to execute
73 endonucleolytic cleavage [21]. The nature of this authorisation signal remains unknown and is
74 particularly intriguing given that, unlike SMG6, neither SMG5 nor SMG7 carry known catalytic activity
75 and are presumed to act as scaffold proteins.
76 PIN domain proteins constitute a widespread family of single-stranded RNA nucleases in prokaryotes
77 and eukaryotes. The canonical PIN core (~120-130 amino acids) adopts a conserved fold – a parallel
78 β-sheet flanked by α-helices – that forms an active site in which typically four acidic residues
79 coordinate one or more divalent metal ions (often Mg^{2+} or Mn^{2+}) to activate water for nucleophilic
80 attack and RNA cleavage [24, 25]. Early structural studies of the human (*Hs*) SMG6 PIN domain [10]
81 identified three key aspartate residues (D1251, D1353, D1392) – a reduced acidic cluster that,
82 although less common within the structurally flexible PIN family, can suffice to support metal-
83 dependent endonucleolytic activity (e.g. [26]). Indeed, *in vitro* assays demonstrated activity of a
84 recombinant wild-type SMG6 PIN domain but not a D1353A mutant [10], and in a mouse model,
85 mutation of two of the three Asp residues yielded effective NMD loss-of-function in vivo [27],
86 validating the critical role of the SMG6 aspartate triade. Intriguingly, SMG5 also carries a C-terminal
87 PIN domain with high similarity to that of SMG6, yet retains only a single conserved Asp (D860 in
88 *Hs*SMG5); consistent with an impaired catalytic site, the recombinant SMG5 PIN domain lacks
89 detectable cleavage activity [10].

90 Here, we investigate the predicted interactions among human SMG5, SMG6 and SMG7. AlphaFold3
91 [28] structure predictions recover the known SMG5-SMG7 interaction via their N-terminal domains
92 and, in addition, predict with high confidence a physical interface between the SMG5 and SMG6 PIN
93 domains that would create a composite active site. In this arrangement, a conserved aspartate from
94 SMG5 (D893) complements the SMG6 aspartate triade to yield the acidic quartet typical of canonical
95 PIN nucleases. We validate these predictions using *in vitro* nuclease assays, showing that the SMG6
96 PIN domain alone has weak nuclease activity that is ~10-fold enhanced in the presence of the SMG5
97 PIN domain. Mutational analyses further identify conserved residues required for activity of the
98 composite PIN configuration. Together, our data provide mechanistic insight into the function of the
99 previously presumed inactive SMG5 PIN domain and suggest a molecular basis for the hypothesised
100 SMG5-dependent authorisation step – namely, complementation of the SMG6 active site.

101 Results

102 Structural models predict a conserved SMG5-SMG6 PIN domain interaction

103 To explore how the metazoan-specific NMD factors SMG5, SMG6, and SMG7 assemble, we
104 performed AlphaFold3 predictions on the full-length human proteins (Figures 1 and S1-S2). The
105 resulting high-confidence model recapitulates as expected the known SMG5-SMG7 complex formed
106 via their N-terminal 14-3-3-like/α-helical domains [18], as well as the established intramolecular
107 complex between the 14-3-3-like and α-helical domain of SMG6 [13] (Figures S1A-B and S2A).
108 Surprisingly however, the model simultaneously predicts a so far unknown complex between the C-
109 terminal PIN domains of SMG5 and SMG6 (Figure 1B). The central interface of this complex is
110 formed by interdigitating helices of both PIN domains (SMG5 α4/5 and SMG6 α8; Figure 1D), while
111 additional mostly hydrophobic contacts are made by N-terminal α-helical extensions of both domains
112 (SMG5 α1 and SMG6 α1; Figure 1E, F). Furthermore, a loop in SMG6 that links its 14-3-3-like and
113 α-helical domain is predicted to fold back onto the central β-sheet of SMG6's PIN domain contributing
114 a further β-strand (SMG6 β1) and forming several backbone hydrogen bonds to the SMG5 PIN
115 domain (Figure 1F). While the central interface of both minimal PIN domains only covers ~70 $Å^2$,
116 these additional contacts increase the putative interaction surface to ~190 $Å^2$. Importantly, this

117 predicted domain arrangement leaves the SMG6 PIN active site completely accessible for substrate
118 RNA and even suggests that SMG5 could contribute catalytically relevant side chains to the
119 ribonuclease center (Figure 1C). To assess evolutionary conservation, we generated analogous
120 predictions for *Drosophila melanogaster* (*Dm*, for SMG5 and SMG6, as no SMG7 is encoded in this
121 organism [29]) and *Caenorhabditis elegans* (*Ce*, whose orthologous proteins are considerably
122 shorter [18]). Both species yielded similar structural configurations, notably preserving the SMG5-
123 SMG6 PIN-PIN interface and the auxiliary SMG5-6 α1 and SMG6 β1 contacts (Figures S1C-F, S2B-
124 C, S3A-B). Consistently, sequence alignments and surface mapping showed strong conservation of
125 interface residues for both SMG5 and SMG6 as well as the predicted SMG6 β1 strand (Figures 2B,
126 C and S3C).

127 **Evolutionary conservation of residues forming a putative composite SMG5-SMG6 active site**

128 The prediction that the SMG5 PIN domain binds in close proximity of the SMG6 PIN active site and
129 could extend several side chains into its catalytic cavity, could suggest that SMG5 contributes to
130 RNA cleavage. To explore the relevance of this model, we compared the resulting active site
131 configuration with other canonical PIN domain family members. According to previous bioinformatic
132 studies [24, 25], the SMG6 PIN domain is most closely related to the PIN of bacterial VapC toxins,
133 which are highly active cytotoxic ribonucleases [26]. Structural superposition of the SMG5-SMG6
134 PIN domain complex with the crystal structure of *Mycobacterium tuberculosis* VapC3 [30]) (Figure
135 2A) reveals that the isolated SMG6 PIN is missing one of the crucial aspartate residues of the
136 catalytic tetrad (*Mt*VapC3: D4, D96, D114, D116 *versus Hs*SMG6: D1251, D1353, D1392, **N**1394).
137 These four Asp residues coordinate the two bivalent active site metal ions (Mg^{2+} or Mn^{2+} in many
138 PIN domains) that are required for activation of a nucleophilic water molecule and stabilization of the
139 pentameric transition state of phosphodiester bond hydrolysis. While the fourth Asp is replaced by
140 Asn in *Hs*SMG6 and *Dm*Smg6, it is even exchanged for an inert glycine residue in *Ce*SMG-6 (Figure
141 S3A, B). Strikingly, association of SMG5 is predicted to supply an additional fully conserved Asp
142 residue (*Hs*SMG5 D893, *Dm*Smg5 D1050, *Ce*SMG-5 D464) in an almost identical position to
143 *Mt*VapC3 D116 that could functionally complement the Asp triad of SMG6. Furthermore, two
144 conserved Lys sidechains of SMG5 (*Hs*SMG5 K896, K897) are predicted to reach into the entry of

145 the active site in sufficient proximity for RNA binding. Their position overlaps with an analogous Arg
146 side chain in VapC3. Together these models, sequence and structural comparisons suggest that
147 SMG5 and SMG6 could form a composite active site with their respective PIN domains that would
148 be catalytically proficient in RNA cleavage.

149 **Mn^{2+}-dependent *in vitro* nuclease activity of SMG6 is enhanced by the SMG5 PIN domain**

150 Based on the above structural predictions, we next sought to validate these experimentally. We first
151 assessed the *in vitro* nuclease activity of the SMG6 PIN domain in the absence and presence of the
152 SMG5 PIN domain. Previous work by Glavan *et al.* used a gel-based assay with a radioactively end-
153 labelled U_{30} RNA oligonucleotide to study SMG6 activity [10]. As a starting point, we developed an
154 analogous fluorescence-based assay using a U_{25} RNA oligonucleotide modified to resist
155 exonucleolytic decay by adding deoxyU residues at both ends and carrying a 6-carboxyfluorescein
156 (6-FAM) label at the 5′ end (Figure 3A). In our standard setup, the probe was incubated at a 1:1
157 molar ratio with recombinant, N-terminally tagged proteins in the presence of Mn^{2+}, and substrate
158 turnover was analysed after 45 min by 10% denaturing urea polyacrylamide gel electrophoresis
159 (PAGE).

160 To examine the role of predicted SMG5-SMG6 interactions, we produced three SMG6 PIN constructs
161 of increasing length (Figure 1A): (i) a minimal PIN domain (aa 1239–1419); (ii) a short extended
162 version (aa 1162–1419) that included the predicted α-helix (α1) and that is termed SMG6 PIN(α ext)
163 in the following; and (iii) a long extended version (aa 567–1419) further comprising the 14-3-3-like
164 and α-helical domains, which the model suggests contact its own PIN domain via a short central β-
165 strand (β1); this protein is termed SMG6 PIN(14-3-3 ext) in the following. The SMG5 construct used
166 throughout (aa 827–1016, termed SMG5 PIN(α ext)) was slightly longer than that of Glavan *et al.*
167 (aa 853–1016; [10]), as it included the predicted α-helical extension adjacent to the core PIN
168 boundary (α1), which according to the structural models interacts with the α-helical SMG6 extension
169 to reinforce the PIN-PIN interface.

170 Side-by-side comparisons revealed that the SMG6 PIN(14-3-3 ext) construct combined with SMG5
171 PIN(α ext) showed the highest activity, yielding near-complete substrate degradation (~95% turnover
172 after 45 min; Figure 3B, lanes 11-12; Figure 3C). Notably, this SMG6 construct also retained basal

173 activity in the absence of SMG5 (~50% turnover; lanes 9-10). The SMG5 construct combined with
174 shorter SMG6 versions showed progressively weaker activity, with the minimal SMG6 PIN (lanes 1-
175 4) and SMG6 PIN(α ext) constructs (lanes 5-8) turning over ~20% and ~30% of substrate,
176 respectively; these SMG6 versions had no significant activity in the absence of SMG5 (Figure 3C).
177 All assays were performed in the presence of Mn^{2+}, the preferred cofactor for many PIN nucleases.
178 Using the SMG5 PIN(α ext)-SMG6 PIN(14-3-3 ext) construct combination, we confirmed cation
179 specificity: substituting Mn^{2+} with Mg^{2+} or Zn^{2+} abolished cleavage, and chelation with EDTA blocked
180 Mn^{2+}-dependent degradation (Figure 3D, E).
181 In summary, we concluded that SMG5 PIN strongly enhances SMG6 PIN activity *in vitro*, and
182 structural extensions on SMG6 contribute to maximal activity.

183 **Extended SMG5-SMG6 contacts can be functionally mimicked by covalent tethering**

184 Our initial interpretation of the higher activity observed with the structurally extended SMG6 construct
185 was that these additional sequences stabilise a PIN-PIN interaction between SMG5 and SMG6 that
186 would otherwise be weak. However, we could not exclude the possibility that the extra SMG6
187 sequences contributed directly to catalysis or RNA binding rather than acting solely as structural
188 stabilisers.
189 To distinguish these possibilities, we used the SMG5 PIN(α ext) and the SMG6 PIN(α ext) constructs,
190 which showed low activity in our assays (Figure 3B, lanes 7-8; Figure 3C), and irreversibly linked
191 them into a single polypeptide using the SpyTag/SpyCatcher system [31]. Remarkably, the covalently
192 tethered SMG5-SMG6 pair displayed much higher activity than the non-tethered proteins; notably,
193 the SpyTag/SpyCatcher version of SMG5 PIN(α ext)-SMG6 PIN(α ext) now resembled in its activity
194 the non-tethered SMG5 PIN(α ext)-SMG6 PIN(14-3-3 ext) proteins (Figure 4A, B). This result
195 supports the idea that the additional SMG6 sequences primarily promote protein-protein interactions
196 and become dispensable when interaction is enforced by other means. In our assay, this was
197 achieved by covalent linkage; *in vivo*, a similar effect may occur through co-recruitment of SMG5
198 and SMG6 to the common binding platform, phospho-UPF1.
199 As a second approach to probe the SMG5-SMG6 interaction, we varied reaction temperature. Our
200 rationale was that temperature exerts opposing effects on two key factors: enzymatic kinetics and

protein-protein interaction. Lower temperatures generally slow catalytic turnover but can stabilise weak interfaces; higher temperatures accelerate intrinsic reaction rates yet destabilise fragile interactions. Thus, if SMG5 and SMG6 interact weakly, we would expect increased activity at low temperature (due to improved complex stability) and reduced activity at high temperature, despite faster kinetics. Conversely, a strongly interacting dimer should show the opposite trend – slower activity at low temperature and faster at high temperature.

We tested this by performing the *in vitro* assay at four temperatures: 0 °C (on ice), 10 °C, 37 °C (as in Figure 3B), and 42 °C (proxy for upper physiological limit in humans). The results were unambiguous: low temperatures strongly favoured substrate turnover by SMG6 variants that were nearly inactive at 37 °C. For example, the SMG6 PIN(α ext) together with SMG5 PIN(α ext) was able to degrade only ~30-40% of substrate at 37 °C–42 °C but 80-90% at 0 °C–10 °C (Figure 4C, lanes 7-8; Figure 4D). Additional observations from the temperature experiment included: (i) even the minimal SMG6 PIN combined with SMG5 gained some activity at 0°C (30-40% turnover; lanes 3-4); and (ii) basal activity of SMG6 PIN proteins alone increased at low temperature as well – for instance, the SMG6 PIN(14-3-3 ext) degraded ~60% at 37 °C but 70-90% at 0 °C–10 °C (lanes 9-10). These effects may reflect improved RNA binding, or stabilisation of protein structure and/or Mn^{2+} coordination at low temperature.

Together, these findings indicate that SMG5-SMG6 PIN domains form a weak interaction that is strongly temperature-sensitive, supporting a model in which extended contacts stabilise the composite active site.

Quantitative comparison of nuclease kinetics through a real-time fluorescent cleavage assay

The gel-based endpoint assays above provided important insights into SMG6 nuclease activity and its modulation by SMG5, but they were unsuitable for kinetic analysis. To enable quantitative measurements, capture early reaction phases, and increase throughput, we developed a fluorescence-based real-time cleavage assay. This platform is particularly advantageous for analysing subtle effects of protein mutations on nuclease activity. We used a variant of the U_{25} RNA oligonucleotide substrate that carried a 6-FAM label at the 5′ end and a Black Hole Quencher 1

228 (BHQ1) at the 3′ end. In the intact oligo, BHQ1 quenches the 6-FAM signal, while cleavage
229 engenders fluorescence (Figure 5A).
230 We benchmarked our assay using conditions similar to the gel-based assay. Reactions were initiated
231 by protein addition, and fluorescence was recorded every minute for 60 min using a plate reader.
232 The assay reproduced all previous findings but allowed precise kinetic comparisons. SMG5 PIN(α
233 ext) + SMG6 PIN(14-3-3 ext) and the SpyTag/SpyCatcher-tethered SMG5-SMG6 pair were highly
234 active, reaching 50% substrate turnover in <5 min (Figure 5B). SMG6 PIN(14-3-3 ext) alone showed
235 clear activity but required >20 min to reach 50% turnover, whereas SMG5 PIN(α ext) + SMG6 PIN(α
236 ext) was very weakly active and all other constructs were inactive.
237 We fitted the fluorescence curves to a single-exponential model to derive rate constants (k_{obs}). The
238 most active constructs yielded k_{obs} values of ~0.2 min^{-1}, whereas SMG6 PIN(14-3-3 ext) alone was
239 almost 7-fold slower ($k_{obs} \approx 0.03$ min^{-1}) (Figure 5C).
240 In summary, this real-time assay enables fine-grain kinetic analysis and provides a robust platform
241 for dissecting SMG5/SMG6 function and mutant phenotypes.

242 **Mutational analysis validates SMG5-contributed active site residues and the SMG5-SMG6**
243 **interaction surface**

244 To validate the structural model, we generated SMG5 and SMG6 mutants targeting two features: the
245 composite active site (Figures 1C and 6A) and the predicted PIN-PIN interface (Figures 1D and 6B).
246 First, we probed the composite active site. Recombinant SMG6 PIN(14-3-3 ext) carrying a D1353A
247 mutation was nucleolytically inactive in all conditions, confirming the essential role of this catalytic
248 residue (Figure 6A, C). On the SMG5 side, converting D893 to alanine abolished the ability of SMG5
249 PIN(α ext) to enhance SMG6-mediated cleavage, consistent with its proposed role in complementing
250 the active site. Furthermore, mutating the conserved K896 and K897 – located near the composite
251 active site and potentially involved in RNA binding – also eliminated SMG5-mediated stimulation.
252 Analogous results were found for these mutants in the SpyTag/SpyCatcher setup (Figure S4A, B).
253 Next, we interrogated the predicted interaction surface. Structural models suggested an electrostatic
254 contact between SMG5 E910 and SMG6 R1396 (Figure 1D). Disrupting this interaction by charge
255 reversal (SMG5 E910R or SMG6 R1396E, together with a WT partner protein) greatly reduced

256 activity (k_{obs} ≈ 0.03 min^{-1} and 0.01 min^{-1}, respectively), compared with that of the two WT proteins
257 (k_{obs} ≈ 0.25 min^{-1}; Figure 6B, D). Strikingly, combining both mutants (SMG5 E901R + SMG6 R1396E)
258 restored activity almost fully (k_{obs} ≈ 0.17 min^{-1}), directly validating the predicted electrostatic
259 interaction. A second interface mutant, SMG6 V1397E, also prevented SMG5-mediated stimulation
260 (Figure S4C-F). Interestingly, both SMG6 interface mutants reduced basal activity even in the
261 absence of SMG5, conceivably because introducing a negative charge (glutamate) near the active
262 site could perturb RNA binding.
263 In summary, these mutational analyses confirm the structural model of active site complementation
264 between SMG5 and SMG6 and identify conserved residues critical for catalysis and PIN–PIN
265 interaction.

266 Discussion

267 The precise roles of SMG5, SMG6, and SMG7 in the effector phase of metazoan NMD have
268 remained unclear for decades. While SMG6 was established as the pathway's dedicated
269 endonuclease, SMG5 and SMG7 were largely considered scaffolds that recruit general decay factors
270 such as deadenylases and decapping enzymes. Our findings challenge this view by demonstrating
271 that SMG5 directly contributes to catalysis: its PIN domain complements the SMG6 active site to
272 form a composite nuclease architecture. This mechanism explains why the isolated SMG6 PIN
273 domain does not trigger mRNA decay in cells even upon tethering [32], why SMG5 acts as a licensing
274 factor for SMG6 [22, 23] and provides a molecular basis for the proposed authorisation step in NMD
275 [21]. Our data together with previous literature, suggests a model in which the SMG5-SMG7
276 heterodimer is recruited efficiently to the phosphorylated C-terminus of UPF1 via its two adjacent 14-
277 3-3-like domains [13, 16, 18, 33, 34], while SMG6 recognizes both the RNA-bound conformation of
278 UPF1 and its phosphorylated N-terminus [13-15]. Only the avidity afforded by this combination of
279 several low affinity interactions brings the two PIN domains of SMG6 and SMG5 into proximity to
280 elicit stable active site formation and RNA cleavage. Furthermore, the intramolecular connection
281 between the 14-3-3-like domain of SMG6 and its PIN domain could ensure that the cut occurs in *cis*
282 in close spatial proximity to the UPF1 RNA binding site and the PTC [12, 35].

283 Composite active sites are not unprecedented in the PIN domain superfamily. Structural studies of
284 bacterial VapC toxins and other PIN-containing effectors have shown that dimerization configures
285 catalytic grooves, often bringing together acidic residues from two domains [26, 36]. Similar
286 principles underlie many PIN-domain and related nucleases, where catalysis is conditional upon
287 oligomerization or conformational change. For instance, CRISPR-associated PIN enzymes can be
288 activated by cyclic tetraadenylate (cA_4)-dependent oligomerization that reconfigures active-site
289 residues across different subunits [37]. Our work extends this paradigm to eukaryotic RNA
290 surveillance, revealing that SMG5 and SMG6 cooperate to assemble a canonical PIN active site that
291 neither domain can fully provide alone.
292 This conditional assembly offers an elegant regulatory strategy. Nuclease activation depends on
293 protein-protein interaction and recruitment to a common platform – phosphorylated [13, 16] and
294 RNA-bound [15] UPF1 – ensuring spatial and temporal control during NMD. The requirement for
295 SMG5-mediated complementation would thus provide a checkpoint for pathway progression, and
296 the catalytic dependency would likely serve as a safeguard against unregulated SMG6 activity in the
297 cytoplasm, thereby preventing indiscriminate RNA cleavage and restricting endonucleolysis to
298 properly assembled NMD complexes.
299 Evolutionary comparisons reinforce this model. *Drosophila melanogaster* lacks SMG7 but retains
300 SMG5 and SMG6 [29], suggesting that the SMG5-SMG6 partnership represents the catalytic core
301 of metazoan NMD. SMG7 may represent an additional, yet dispensable adaptor to enhance
302 exonucleolytic decay or pathway regulation, whereas SMG5's contribution to SMG6 activation
303 appears indispensable. This observation underscores that SMG5 is not merely a scaffold but a
304 critical licensing factor for SMG6 endonucleolytic activity.
305 Beyond clarifying SMG5's role, these findings highlight composite PIN architectures as a recurring
306 evolutionary solution for licensing nuclease activity. Conditional assembly allows organisms to
307 balance catalytic potency with specificity, a principle that may apply broadly to RNA decay pathways
308 and other nucleases. Future work should address whether SMG7 contributes additional regulatory
309 layers, how UPF1 phosphorylation dynamics influence composite active site formation, and whether
310 similar composite architectures exist in other metazoan RNA surveillance systems. Understanding

311 these mechanisms will not only refine models of NMD regulation but may also inform therapeutic
312 strategies targeting aberrant RNA decay in genetic disease and cancer.

313 Methods

314 Cloning

315 Human *SMG5* and *SMG6* sequences were amplified by PCR from plasmids pcDNA3.1-MS2-HA-
316 HsSmg5_T (Addgene #147552) [19] and pCIneo-λN-HA-HsSmg6_I (Addgene #146551) [38], or
317 from HEK293 cell cDNA, and then cloned by Golden-gate cloning into low-copy plasmid pLIBT7 in
318 fusion with N-terminal His-tag (for SMG5), N-terminal HisGST-tag (for SMG6), N-terminal SpyTag
319 [31] and C-terminal His-tag (for SMG5) or N-terminal SpyCatcher [31] and C-terminal His-tag (for
320 SMG6). For bacterial co-expression, SMG5 plasmids carried ampicillin resistance and SMG6
321 plasmids kanamycin resistance. To generate specific amino acid mutations, we used the classical
322 QuikChange site-directed mutagenesis protocol based on polymerase chain reaction (PCR)
323 amplification using *Pfu*Turbo DNA polymerase (Agilent) and two complementary oligonucleotide
324 primers (Microsynth) containing the desired mutation. Following temperature cycling, reactions were
325 treated with *Dpn*I (New England Biolabs) for digestion of parental DNA template. After transformation
326 (XL2-Blue), positive clones were identified and validated by Sanger sequencing. Oligos used for
327 mutagenesis are as follows, with lowercase letters indicating mutated nucleotides:

Protein	Mutation	Oligo sequences (5' to 3'), upper and lower oligos
SMG5	D893A	CCCAAGGACAGTGATCGATGGgCTagctTTGCTGAAGAAGGAACACCCAG CTGGGTGTTCCTTCTTCAGCAAagctAGcCCATCGATCACTGTCCTTGGG
SMG5	E910R	GGGATTCGGTACCTGcgcGCAGAGTTTAAAAAAGGAAAC GTTTCCTTTTTTAAACTCTGCgcgCAGGTACCGAATCCC
SMG5	K896A,K897A	GATGGCCTGGATTTGCTGgctgcaGAACACCCAGGGGCCCGG CCGGGCCCCTGGGTGTTCtgcagcCAGCAAATCCAGGCCATC
SMG6	D1353A	GGCCAGCTGGGTAACAACGcaGATCTCATCCTGTCCTGCT GCAGGACAGGATGAGATCtgCGTTGTTACCCAGCTGGC
SMG6	R1396E	GACGGATGACCGGAACCTcgagGTGAAGGCGCTCACAAG CTTGTGAGCGCCTTCACctcgAGGTTCCGGTCATCCGTC
SMG6	V1397E	CGGAACCTGCGTGagAAGGCGCTCACAAGGAA TTCCTTGTGAGCGCCTTctCACGCAGGTTCCG

328 The overall list of DNA constructs used in this study is as follows:

329 pLIBT7_A_HisHsSMG5(827-C)

330 pLIBT7_A_HisHsSMG5(827-C)_D893A

331 pLIBT7_A_HisHsSMG5(827-C)_E910R

332 pLIBT7_A_HisHsSMG5(827-C)_K896A, K897A

333 pLIBT7_A_SpyTag-SMG5(827-C)-His

334 pLIBT7_A_SpyTag-SMG5(827-C)-His_D893A

335 pLIBT7_A_SpyTag-SMG5(827-C)-His_K896A, K897A

336 pLIBT7_K_HisGST-TEV-SMG6(1162-C)

337 pLIBT7_K_HisGST-TEV-SMG6(567-C)

338 pLIBT7_K_HisGST-TEV-SMG6(567-C)_D1353A

339 pLIBT7_K_HisGST-TEV-SMG6(567-C)_R1396E

340 pLIBT7_K_HisGST-TEV-SMG6(567-C)_V1397E

341 pLIBT7_K_SpyCatcher-SMG6(1162-C)-His

342 pLIBT7_K_SpyCatcher-SMG6(1162-C)-His_D1353A

343 pLIBT7_K_SpyCatcher-SMG6(1162-C)-His_V1397E

344 **Expression, and purification of SMG5 and SMG6 proteins**

345 Pairs of SMG5- and SMG6-expression plasmids were co-transformed into electrocompetent *E. coli*
346 Rosetta(DE3) cells and positive clones were selected on LB plates supplemented with 100 µg/mL
347 ampicillin, 50 µg/mL kanamycin, and 30 µg/mL chloramphenicol. These cells were used to inoculate
348 1 L cultures in TB medium, and after growth at 37 °C to an OD600 of 0.5-1 the temperature was
349 reduced to 22 °C. Expression was then induced by addition of IPTG to a final concentration of
350 0.4 mM, and the cultures were left shaking at 22 °C overnight (16 h). Bacteria were collected by
351 centrifugation and the pellet was resuspended in 70 mL of Lysis buffer (50 mM Tris-HCl pH 7.5,
352 300 mM NaCl, 5% glycerol, 25 mM imidazole) supplemented with 5 mM β-mercaptoethanol and
353 protease inhibitors (Roche). Cells were lysed by sonication on ice (Bandelin sonicator equipped with
354 VS70T-tip) for 12 min total sonication time (40% output, pulsing 1 s ON / 1 s OFF) and the lysate
355 was clarified by centrifugation at 40000× *g* at 4 °C for 30 min. This lysate was then loaded on a 5 mL
356 HisTrap-HP column (Cytiva) equilibrated in Lysis buffer, followed by a 6 column volume (cV) wash
357 with Lysis buffer. Bound material was then eluted with a 10 cV gradient from Lysis buffer to the same
358 buffer supplemented with 500 mM imidazole. His-GST-TEV-SMG6 and His-SMG5 proteins eluted in

359 separate but overlapping peaks, indicating that their interaction was too weak to fully withstand this
360 purification at 300 mM NaCl concentration. Fractions containing the desired proteins were
361 nevertheless pooled, concentrated to a volume of around 500 µL, and injected onto a Superdex200
362 Increase size-exclusion column equilibrated in SEC buffer (20 mM Tris-HCl pH 7.5, 250 mM NaCl).
363 His-GST-TEV-SMG6 and His-SMG5 proteins eluted in distinct peaks, which were individually pooled
364 and concentrated. The obtained protein solutions were aliquoted, snap-frozen in liquid nitrogen, and
365 stored at -70 °C.

366 **Expression and purification of SpyTag-SMG5/SpyCatcher-SMG6 pairs**

367 Combinations of the desired plasmid were co-transformed into *E. coli* Rosetta(DE3) and cultures
368 were grown and lysed as described above. After loading on a His-Trap column the dimer eluted
369 slightly separated from excess SpyTag-SMG5 protein, and fractions containing the desired dimer
370 were concentrated to 500 µL followed by Superdex200 Increase size-exclusion chromatography as
371 described above. The dimer eluted well-separated from the remaining excess SpyTag-SMG5 protein,
372 and was concentrated, aliquoted, snap-frozen and stored at -70 °C.

373 ***In vitro* gel-based nuclease assay**

374 In a reaction volume of 5 µL, 3 µM of 5'-6FAM-dU-U_{25}-dU-oligo (IDT) was incubated with 3 µM of
375 recombinant proteins in reaction buffer containing 100 mM NaCl, 10% glycerol, 5 mM $MnCl_2$, 25 mM
376 Tris-HCl pH 7.5, 1 mM DTT. In some assays (e.g., to show the specificity of Mn^{2+}-based RNA
377 degradation) 1 mM EGTA and/or 30 mM EDTA were added. The reaction mix was then incubated at
378 temperatures indicated in figure legends (42 °C, 37 °C, 10 °C, or 0 °C), for a reaction time of 45 min
379 (or for 0 min for control sample). After incubation, each reaction was first mixed with 5 µL of 2x RNA
380 loading dye (95% formamide, 18 mM EDTA, 0.025% SDS, and Bromophenol Blue), then heated at
381 95 °C for 5 min, chilled on ice, then loaded on a 10% polyacrylamide gel containing 7 M Urea
382 (Invitrogen, EC68755BOX). Gel electrophoresis was performed at 120 V for 50 min.

383 ***In vitro* kinetic nuclease assay**

384 Using substrate concentration of 3 µM for the fluorescence-quenched oligo 5'-6FAM-dU-U_{25}-dU-3'-
385 BHQ1 (IDT) and 3 µM of recombinant proteins (or RNase-free water as negative control), reactions

386 were carried out in 10 µL and reaction buffer 100 mM NaCl, 10% glycerol, 5 mM $MnCl_2$, 1 mM EGTA,
387 25 mM Tris-HCl pH 7.5, 1 mM DTT. To catch early reaction timepoints reliably, reactions were
388 typically started by adding the proteins as the last component. The reaction was then incubated at
389 25 °C for 60 min in a flat-bottom black 384-well plate (Corning). Fluorescence signal was measured
390 every minute in a plate reader (Tecan Safire 2). To calculate observed reaction rate constants (k_{obs}),
391 within one experiment (i.e., on the same plate) raw data were first normalised to 0-100%, followed
392 by non-linear curve fit (single exponential growth to plateau, using GraphPad Prism 10 software)
393 with formula $Y=100 * (1 - \exp(-k_{obs} * X))$. As we noted that bleaching of signal occurred over time
394 (i.e., 100% signal decays), we also tried curve fit formulas with a bleaching term, but as the obtained
395 k_{obs} values were near-identical to the simple fits, we report the outcomes from the simple model in
396 this study.

397 **Structure predictions**

398 AlphaFold3 [28] was used for structure predictions (5 models each) of complexes formed by full
399 length human (*Hs*) SMG5-6-7, *Drosophila melanogaster* (*Dm*) Smg5-6 (no Smg7 ortholog present
400 in flies), or *Caenorhabditis elegans* (*Ce*) SMG-5-6-7 each including U_6 RNA and 2 Mg^{2+}. The highest
401 ranked model of each prediction was used for visualizations with ChimeraX1.10 [39]. Predicted
402 Aligned Error (PAE) plots were generated with PAE viewer [40], while surface conservation scores
403 were calculated using ConSurf [41] with structure models as input and default settings.

404 **Sequence alignments**

405 Sequences of human SMG5, SMG6 and orthologous proteins were identified via TreeFam [42] or by
406 BLAST search [43] and aligned using the MUSCLE webserver [44] from within JALVIEW [45].
407 Positional conservation and similarity scores were calculated using the ESPRIPT webserver [46]
408 with default settings.

409 CRediT authorship contribution statement

410 **Enes S. Arpa**: Writing – review & editing, Writing – original draft, Visualization, Validation,
411 Conceptualization, Formal analysis, Investigation, Methodology. **Michael Taschner:** Writing –
412 review & editing, Writing – original draft, Conceptualization, Investigation, Methodology. **Mara De**

Matos: Investigation, Methodology. **Stefanie Jonas:** Writing – review & editing, Writing – original draft, Visualization, Funding acquisition, Conceptualization, Methodology, Supervision. **David Gatfield:** Writing – review & editing, Writing – original draft, Visualization, Funding acquisition, Conceptualization, Formal analysis, Supervision, Project administration.

Declaration of competing interest

The authors declare that they have no known competing financial interests or personal relationships that could have appeared to influence the work reported in this paper.

Acknowledgements

This work was supported by the University of Lausanne and ETH Zurich, Swiss National Science Foundation (SNSF) NCCR RNA & Disease Phase III funding (grant number 205601 to D.G. and S.J.), SNSF Project funding (grant number 212423 to D.G., and 207458 to S.J.), an ERC Consolidator grant funded via SERI (MB22.00064 to S.J.), an EMBO Young Investigators Award (4918 to S.J.).

426 ## References

427 [1] Peltz SW, Brown AH, Jacobson A. mRNA destabilization triggered by premature translational
428 termination depends on at least three cis-acting sequence elements and one trans-acting factor.
429 *Genes & Development*. 1993;7:1737-54.

430 [2] Leeds P, Peltz SW, Jacobson A, Culbertson MR. The product of the yeast UPF1 gene is required
431 for rapid turnover of mRNAs containing a premature translational termination codon. *Genes &*
432 *Development*. 1991;5:2303-14.

433 [3] Hodgkin J, Papp A, Pulak R, Ambros V, Anderson P. A new kind of informational suppression in
434 the nematode Caenorhabditis elegans. *Genetics*. 1989;123:301-13.

435 [4] He F, Jacobson A. Upf1p, Nmd2p, and Upf3p regulate the decapping and exonucleolytic
436 degradation of both nonsense-containing mRNAs and wild-type mRNAs. *Molecular and Cellular*
437 *Biology*. 2001;21:1515-30.

438 [5] Lejeune F, Li X, Maquat LE. Nonsense-mediated mRNA decay in mammalian cells involves
439 decapping, deadenylating, and exonucleolytic activities. *Molecular Cell*. 2003;12:675-87.

440 [6] Karousis ED, Muhlemann O. The broader sense of nonsense. Trends in biochemical sciences.
441 2022;47:921-35.

442 [7] Muhlrad D, Parker R. Premature translational termination triggers mRNA decapping. *Nature*.
443 1994;370:578-81.

444 [8] Mitchell P, Tollervey D. An NMD pathway in yeast involving accelerated deadenylation and
445 exosome-mediated 3'-->5' degradation. *Molecular Cell*. 2003;11:1405-13.

446 [9] Gatfield D, Izaurralde E. Nonsense-mediated messenger RNA decay is initiated by
447 endonucleolytic cleavage in Drosophila. *Nature*. 2004;429:575-8.

448 [10] Glavan F, Behm-Ansmant I, Izaurralde E, Conti E. Structures of the PIN domains of SMG6 and
449 SMG5 reveal a nuclease within the mRNA surveillance complex. *The EMBO Journal*.
450 2006;25:5117-25.

451 [11] Huntzinger E, Kashima I, Fauser M, Sauliere J, Izaurralde E. SMG6 is the catalytic endonuclease
452 that cleaves mRNAs containing nonsense codons in metazoan. *RNA*. 2008;14:2609-17.

453 [12] Eberle AB, Lykke-Andersen S, Muhlemann O, Jensen TH. SMG6 promotes endonucleolytic
454 cleavage of nonsense mRNA in human cells. *Nature Structural & Molecular Biology*. 2009;16:49-
455 55.
456 [13] Chakrabarti S, Bonneau F, Schussler S, Eppinger E, Conti E. Phospho-dependent and phospho-
457 independent interactions of the helicase UPF1 with the NMD factors SMG5-SMG7 and SMG6.
458 *Nucleic Acids Research*. 2014;42:9447-60.
459 [14] Barbarin-Bocahu I, Ulryck N, Rigobert A, Ruiz Gutierrez N, Decourty L, Raji M, et al. Structure
460 of the Nmd4-Upf1 complex supports conservation of the nonsense-mediated mRNA decay
461 pathway between yeast and humans. *PLoS Biology*. 2024;22:e3002821.
462 [15] Langer LM, Kurscheidt K, Basquin J, Bonneau F, Iermak I, Basquin C, et al. UPF1 helicase
463 orchestrates mutually exclusive interactions with the SMG6 endonuclease and UPF2. *Nucleic*
464 *Acids Research*. 2024;52:6036-48.
465 [16] Okada-Katsuhata Y, Yamashita A, Kutsuzawa K, Izumi N, Hirahara F, Ohno S. N- and C-terminal
466 Upf1 phosphorylations create binding platforms for SMG-6 and SMG-5:SMG-7 during NMD.
467 *Nucleic Acids Research*. 2012;40:1251-66.
468 [17] Unterholzner L, Izaurralde E. SMG7 acts as a molecular link between mRNA surveillance and
469 mRNA decay. *Molecular Cell*. 2004;16:587-96.
470 [18] Jonas S, Weichenrieder O, Izaurralde E. An unusual arrangement of two 14-3-3-like domains in
471 the SMG5-SMG7 heterodimer is required for efficient nonsense-mediated mRNA decay. *Genes*
472 *& Development*. 2013;27:211-25.
473 [19] Loh B, Jonas S, Izaurralde E. The SMG5-SMG7 heterodimer directly recruits the CCR4-NOT
474 deadenylase complex to mRNAs containing nonsense codons via interaction with POP2. *Genes*
475 *& Development*. 2013;27:2125-38.
476 [20] Colombo M, Karousis ED, Bourquin J, Bruggmann R, Muhlemann O. Transcriptome-wide
477 identification of NMD-targeted human mRNAs reveals extensive redundancy between SMG6-
478 and SMG7-mediated degradation pathways. *RNA*. 2017;23:189-201.

479 [21] Boehm V, Kueckelmann S, Gerbracht JV, Kallabis S, Britto-Borges T, Altmuller J, et al. SMG5-
480 SMG7 authorize nonsense-mediated mRNA decay by enabling SMG6 endonucleolytic activity.
481 *Nature Communications*. 2021;12:3965.
482 [22] Huth M, Santini L, Galimberti E, Ramesmayer J, Titz-Teixeira F, Sehlke R, et al. NMD is required
483 for timely cell fate transitions by fine-tuning gene expression and regulating translation. *Genes*
484 *& Development*. 2022;36:348-67.
485 [23] Viscardi MJ, Sehgal E, Arribere JA. Endonucleolytic cleavage is the primary mechanism of
486 decay elicited by C. elegans nonsense-mediated mRNA decay. Genome research.
487 2025;35:1337-48.
488 [24] Senissar M, Manav MC, Brodersen DE. Structural conservation of the PIN domain active site
489 across all domains of life. *Protein Sci*. 2017;26:1474-92.
490 [25] Matelska D, Steczkiewicz K, Ginalski K. Comprehensive classification of the PIN domain-like
491 superfamily. *Nucleic Acids Research*. 2017;45:6995-7020.
492 [26] Arcus VL, McKenzie JL, Robson J, Cook GM. The PIN-domain ribonucleases and the
493 prokaryotic VapBC toxin-antitoxin array. *Protein Eng Des Sel*. 2011;24:33-40.
494 [27] Katsioudi G, Dreos R, Arpa ES, Gaspari S, Liechti A, Sato M, et al. A conditional Smg6 mutant
495 mouse model reveals circadian clock regulation through the nonsense-mediated mRNA decay
496 pathway. *Sci Adv*. 2023;9:eade2828.
497 [28] Abramson J, Adler J, Dunger J, Evans R, Green T, Pritzel A, et al. Accurate structure prediction
498 of biomolecular interactions with AlphaFold 3. *Nature*. 2024;630:493-500.
499 [29] Gatfield D, Unterholzner L, Ciccarelli FD, Bork P, Izaurralde E. Nonsense-mediated mRNA
500 decay in Drosophila: at the intersection of the yeast and mammalian pathways. *The EMBO*
501 *Journal*. 2003;22:3960-70.
502 [30] Das U, Pogenberg V, Subhramanyam UK, Wilmanns M, Gourinath S, Srinivasan A. Crystal
503 structure of the VapBC-15 complex from Mycobacterium tuberculosis reveals a two-metal ion
504 dependent PIN-domain ribonuclease and a variable mode of toxin-antitoxin assembly. *J Struct*
505 *Biol*. 2014;188:249-58.

506 [31] Zakeri B, Fierer JO, Celik E, Chittock EC, Schwarz-Linek U, Moy VT, et al. Peptide tag forming
507 a rapid covalent bond to a protein, through engineering a bacterial adhesin. *Proceedings of the*
508 *National Academy of Sciences of the United States of America*. 2012;109:E690-7.
509 [32] Nicholson P, Josi C, Kurosawa H, Yamashita A, Muhlemann O. A novel phosphorylation-
510 independent interaction between SMG6 and UPF1 is essential for human NMD. *Nucleic Acids*
511 *Research*. 2014;42:9217-35.
512 [33] Fukuhara N, Ebert J, Unterholzner L, Lindner D, Izaurralde E, Conti E. SMG7 is a 14-3-3-like
513 adaptor in the nonsense-mediated mRNA decay pathway. *Molecular Cell*. 2005;17:537-47.
514 [34] Durand S, Franks TM, Lykke-Andersen J. Hyperphosphorylation amplifies UPF1 activity to
515 resolve stalls in nonsense-mediated mRNA decay. Nature communications. 2016;7:12434.
516 [35] Boehm V, Haberman N, Ottens F, Ule J, Gehring NH. 3' UTR length and messenger
517 ribonucleoprotein composition determine endocleavage efficiencies at termination codons. *Cell*
518 *Reports*. 2014;9:555-68.
519 [36] Cook GM, Robson JR, Frampton RA, McKenzie J, Przybilski R, Fineran PC, et al. Ribonucleases
520 in bacterial toxin-antitoxin systems. *Biochimica et Biophysica Acta*. 2013;1829:523-31.
521 [37] Wang F, Zhao P, Bi X, Zheng R, Tian X, Xu J, et al. Cyclic tetraadenylate binding induces
522 dimerization of protein dimers to activate a CRISPR-associated PIN nuclease. *Nucleic Acids*
523 *Research*. 2025;53.
524 [38] Kashima I, Jonas S, Jayachandran U, Buchwald G, Conti E, Lupas AN, et al. SMG6 interacts
525 with the exon junction complex via two conserved EJC-binding motifs (EBMs) required for
526 nonsense-mediated mRNA decay. *Genes & Development*. 2010;24:2440-50.
527 [39] Meng EC, Goddard TD, Pettersen EF, Couch GS, Pearson ZJ, Morris JH, et al. UCSF ChimeraX:
528 Tools for structure building and analysis. *Protein Sci*. 2023;32:e4792.
529 [40] Elfmann C, Stulke J. PAE viewer: a webserver for the interactive visualization of the predicted
530 aligned error for multimer structure predictions and crosslinks. *Nucleic Acids Research*.
531 2023;51:W404-W10.
532 [41] Yariv B, Yariv E, Kessel A, Masrati G, Chorin AB, Martz E, et al. Using evolutionary data to make
533 sense of macromolecules with a "face-lifted" ConSurf. *Protein Sci*. 2023;32:e4582.

534 [42] Ruan J, Li H, Chen Z, Coghlan A, Coin LJ, Guo Y, et al. TreeFam: 2008 Update. *Nucleic Acids*
535 *Research*. 2008;36:D735-40.
536 [43] Altschul SF, Madden TL, Schaffer AA, Zhang J, Zhang Z, Miller W, et al. Gapped BLAST and
537 PSI-BLAST: a new generation of protein database search programs. *Nucleic Acids Research*.
538 1997;25:3389-402.
539 [44] Edgar RC. MUSCLE: multiple sequence alignment with high accuracy and high throughput.
540 *Nucleic Acids Research*. 2004;32:1792-7.
541 [45] Waterhouse AM, Procter JB, Martin DM, Clamp M, Barton GJ. Jalview Version 2--a multiple
542 sequence alignment editor and analysis workbench. Bioinformatics. 2009;25:1189-91.
543 [46] Robert X, Gouet P. Deciphering key features in protein structures with the new ENDscript server.
544 *Nucleic Acids Research*. 2014;42:W320-4.
545
546

547 ## Figure Legends

548 **Figure 1. Structure models of SMG5 and SMG6 predict formation of a composite PIN domain.**
549 (**A**) Schematic domain architecture of *Hs*SMG5 and SMG6. The constructs used in the study, i.e.
550 SMG5 PIN(α extension) (827-C), SMG6 PIN(minimal) (1239-C), SMG6 PIN(α extension) (1162-C)
551 and SMG6 PIN(14-3-3 extension) (567-C), are indicated at the bottom of each cartoon. The α-helices
552 located N-terminally to the PIN domains that are predicted to interact are highlighted in colour and
553 labelled α1. The β-strand, which is inserted in a loop between SMG6 14-3-3-like (14-3-3) and α-
554 helical (αH) domain and which is predicted to intramolecularly complement the PIN-domain β-sheet
555 is indicated as β1.
556 (**B**) Model of the complex between *Hs*SMG5 PIN domain (purple, pink) and the folded domains of
557 *Hs*SMG6 (shades of green) based on an AlphaFold3 model of the *Hs*SMG5-6-7 complex with U_6-
558 RNA and 2 Mg^{2+}. Domains are coloured as in (A). RNA (grey) and metal ions (yellow spheres) in the
559 active site are shown. Elements that contribute to the interaction i.e. α1-helices and β1-strand are
560 highlighted and labelled.
561 (**C**) Zoom into the proposed composite active site. Active site residues of SMG6 (green) and SMG5
562 (purple) are shown as sticks and labelled. Residues mutated in this study are underlined. Predicted
563 positions of two bivalent cations (M^{2+}) that are coordinated by the acidic residues, as well as three
564 nucleotides of RNA substrate (dark grey) are also shown. Dotted lines indicate putative hydrogen
565 bonds and salt bridges.
566 (**D**) Zoom into the *Hs*SMG5PIN-SMG6PIN interface viewed from the bottom of the active site shown
567 in (C). Residues of SMG5 (purple) and SMG6 (green) that are predicted to contribute to binding are
568 shown as sticks and labelled. Residues mutated in the study are underlined. Dotted lines indicate
569 putative hydrogen bonds or salt bridges.
570 (**E**) Predicted interface between α-helical extensions (α1) of *Hs*SMG5 (pink) and SMG6 (light green)
571 PIN domains. Interface residues are shown as sticks and labelled.
572 (**F**) Predicted interface between SMG6 α1 (light green) and β1 with SMG5PIN (purple). Dotted lines
573 indicate putative hydrogen bonds or salt bridges.

574 **Figure 2. The composite SMG5-6 PIN active site and domain interface are evolutionarily**
575 **conserved.**
576 (**A**) Superposition of the crystal structure of prototypical PIN domain family member *Mt*VapC3 (light
577 grey, PDB ID 4CHG)[30] shows that it displays a similar arrangement of active site residues as the
578 composite SMG5-6 PIN domain. Active site residues are shown as sticks and labelled. The two metal
579 ions crystallized with VapC (Mn^{2+}, Mg^{2+}) are shown as grey spheres.
580 (**B**) Surface conservation of the SMG5 (purple) and SMG6 (green) PIN domain interface, with
581 increasing color darkness corresponding to increased conservation.
582 (**C**) Sequence alignment of the extended SMG6 PIN domain including β1 strand and α1 helix.
583 Orthologs from *Homo sapiens* (*Hs*), *Mus musculus* (*Mm*), *Gallus gallus* (*Gg*), *Xenopus tropicalis* (*Xt*),
584 *Danio rerio* (*Dr*), *Strongylocentrotus purpuratus* (*Sp*, Purple urchin), *Drosophila melanogaster* (*Dm*)
585 and *Caenorhabditis elegans* (*Ce*) are compared, and residues with complete conservation and 70%
586 similarity are highlighted in dark and light green, respectively. Predicted secondary structure
587 elements of *Hs* and *Ce* proteins are denoted above and below the alignment, respectively. Residues
588 involved in the predicted SMG5 interface (purple), active site metal coordination (yellow) and RNA
589 substrate binding (grey) are indicated by circles above the alignment. Red stars mark amino acids
590 that were mutated in this study, while red borders mark residues that correspond to VapC active site
591 components.

592 **Figure 3. SMG5-PIN and SMG6-PIN together degrade RNA in a Mn^{2+} dependent manner.**
593 (**A**) Schematic of the gel-based *in vitro* RNA degradation assay using 5'-6FAM-conjugated RNA oligo
594 (5'-6FAM-deoxyU-U_{25}-deoxyU-3').
595 (**B**) Cleavage assay using 3 μM 5'-6FAM RNA oligo incubated with 3 μM of the indicated protein
596 constructs in 5 μL of reaction buffer (100 mM NaCl, 5 mM $MnCl_2$, 1 mM DTT, 10% glycerol, 25 mM
597 Tris-HCl pH 7.5) for 45 min (or 0 min for controls) at 37 °C. Reactions were run on 10% PAGE-Urea
598 gels. The bands corresponding to intact substrate and decay products are indicated.
599 (**C**) Quantification of RNA gel degradation assay from (C) and from three additional replicates of
600 identical experiments. The amount of remaining probe (upper band) with regard to the 0 min

601 timepoint (=100%) was quantified. Data are plotted as means ± SD. *P*-values were calculated using
602 two-tailed unpaired *t*-test.
603 (**D**) Similar to experiment shown in panel (C), 3 μM of substrate and 3 μM of indicated protein con-
604 structs were incubated with either 5 mM $MnCl_2$, $MgCl_2$, or $ZnCl_2$ in a 5 μL reaction volume (buffer
605 conditions: 100 mM NaCl, 1 mM EGTA, 1 mM DTT, 10% glycerol, 25 mM Tris-HCl pH 7.5). After
606 0 min and 45 min at 37 °C, reactions were analysed by PAGE. 30 mM EDTA (last 3 lanes) was used
607 to show the specificity of Mn^{2+}-mediated RNA degradation.
608 (**E**) Quantification of degradation assay shown in (E).

609 **Figure 4. Covalent tethering and low temperature stabilize weak SMG5-SMG6 PIN domain**
610 **interaction to enhance catalytic activity.**
611 (**A**) Cleavage assay using 3 μM 5'-6FAM RNA oligo incubated with 3 μM of the indicated protein
612 constructs in 5 μL of reaction buffer (100 mM NaCl, 5 mM $MnCl_2$, 1 mM DTT, 10% glycerol, 25 mM
613 Tris-HCl pH 7.5) for 45 min (or 0 min for controls) at 37 °C. Reactions were run on 10% PAGE-Urea
614 gels. Lanes 13 and 14 show the covalently tethered SMG5 PIN(α extension) and SMG6 PIN(α ex-
615 tension), using the SpyTag/SpyCatcher strategy.
616 (**B**) Quantification of RNA gel degradation assay from (A) and from three additional replicates of
617 identical experiments. The amount of remaining probe (upper band) with regard to the 0 min
618 timepoint (=100%) was quantified. Data are plotted as means ± SD. *P*-values were calculated using
619 two-tailed unpaired *t*-test. Note that apart from the values in lanes 13 and 14 – showing the
620 SpyTag/SpyCatcher-tethered SMG5-SMG6 pair – this graph reports on the same experimental data
621 as in Figure 3 (B) for lanes 1-12.
622 (**C**) As in (A), yet with experiments carried out at reaction temperatures of 42, 37, 10, or 0 °C.
623 (**D**) Quantification of the assay shown in (C).

624 **Figure 5. Real-time fluorescent cleavage assay reveals kinetic differences among SMG5-**
625 **SMG6 constructs.**
626 (**A**) Schematic of the real-time fluorescent cleavage assay using the 5'-6FAM-dU-U_{25}-dU-3'-BHQ1
627 substrate (termed 5'-6FAM-3'-BHQ1 in remainder of figure legends).

628 (**B**) 3 μM 5'-6FAM-3'-BHQ1 oligo were incubated with 3 μM of the indicated protein constructs (or
629 RNase-free water, as control) in 10 μL volume (reaction buffer: 100 mM NaCl, 5 mM $MnCl_2$, 1 mM
630 EGTA, 1 mM DTT, 10% glycerol, 25 mM Tris-HCl pH 7.5) for 60 min at 25 °C, with measurements at
631 1 min interval in a plate reader. Raw fluorescence values were plotted for each reaction (each con-
632 dition run in triplicates) as medians ± SD.
633 (**C**) Observed rate constants (k_{obs}) calculated from each sample shown in (B). Data are plotted as
634 means ± SD. The *P*-values were calculated using two-tailed unpaired *t*-test.

635 **Figure 6. Mutational analysis confirms composite active site and PIN-PIN interface in SMG5-**
636 **SMG6 complex.**
637 (**A**) 3 μM 5'-6FAM-3'-BHQ1 oligo were incubated with 3 μM of the indicated protein constructs that
638 probe the catalytic site residues and its environment (SMG5 D893A, K896A, K897A and SMG6
639 D1353A) in 10 μL volume (reaction buffer: 100 mM NaCl, 5 mM $MnCl_2$, 1 mM EGTA, 1 mM DTT,
640 10% glycerol, 25 mM Tris-HCl pH 7.5) for 60 min at 25 °C, with measurements at 1 min interval in a
641 plate reader. Raw fluorescence values were plotted for each reaction (each condition run in tripli-
642 cates) as averages with error bars corresponding to ± SD.
643 (**B**) Identical to (A), but for mutants that probe the interaction interface (SMG5 E910R, SMG6
644 R1396E).
645 (**C**) Observed rate constants (k_{obs}) calculated from each sample shown in (A). Data are plotted as
646 means ± SD. The *P*-values were calculated using two-tailed unpaired *t*-test.
647 (**D**) As in (C), for data shown in (B).

648 **Supplementary Figures**

649 **Figure S1. Structural predictions of SMG5-6-7 complexes across evolution. Related to Figures**
650 **1, 2 and S2.**

651 (**A**) AlphaFold3 model of the full-length *Hs*SMG5-6-7 complex with U_6 RNA and 2 Mg^{2+} (ipTM=0.41,
652 pTM=0.46). Intra- and intermolecular complexes that were predicted with high confidence (expected
653 position error ≤5Å) are highlighted in purple (extended SMG5-6PIN domains complex), blue (SMG5-
654 7 14-3-3/α-helical domains complex) and chartreuse (SMG6 14-3-3/α-helical domains).

655 (**B**) Predicted Aligned Error (PAE = expected position error) plot for the model in (A). Coloured
656 outlines mark structural domains and complexes with high predicted likelihoods corresponding to
657 (A).

658 (**C**) AlphaFold3 model of the full-length *Dm*Smg5-6 complex with U_6 RNA and 2 Mg^{2+} (ipTM=0.48,
659 pTM=0.42). Intra- and intermolecular complexes that were predicted with high confidence (PAE ≤5Å)
660 are highlighted in purple (extended SMG5-6PIN domains complex), blue (SMG5 14-3-3/α-helical
661 domains) and chartreuse (SMG6 14-3-3/α-helical domains).

662 (**D**) PAE plot for the model in (C). Coloured outlines mark structural domains and complexes with
663 high predicted likelihoods corresponding to (C).

664 (**E**) AlphaFold3 model of the full-length *Ce*SMG-5-6-7 complex with U_6 RNA and 2 Mg^{2+} (ipTM=0.37,
665 pTM=0.46).

666 (**F**) Intra- and intermolecular complexes that were predicted with high confidence (PAE ≤5Å) are
667 highlighted in purple (extended SMG5-6PIN domains complex), blue (SMG5 14-3-3/α-helical
668 domains complex) and chartreuse (SMG6 14-3-3/α-helical domains).

669 **Figure S2. Local confidence of AlphaFold3 models. Related to Figures 1, 2 and S1.**

670 (**A**) Predicted local distance difference test (pLDDT) values per residue for the AlphaFold3 model of
671 the *Hs*SMG5-6-7 – RNA – Mg^{2+} complex. pLDDT scores from 100-0 are coloured in gradients for
672 SMG5 (from dark purple to light blue), SMG6 (from dark to light green), SMG7 (from dark orange to
673 light yellow), and RNA (from black to white). Structures are oriented as in Figure S1 (A).

674 (**B**) pLDDT values per residue for the AlphaFold3 model of the *Dm*Smg5-6 – RNA – Mg^{2+} complex.
675 pLDDT scores from 100-0 are coloured in gradients analogous to (A). Orientation of the model as in
676 Figure S1 (C).
677 (**C**) pLDDT values per residue for the AlphaFold3 model of the *Ce*SMG-5-6-7 – RNA – Mg^{2+} complex.
678 pLDDT scores from 100-0 are coloured in gradients analogous to (A). Model orientations correspond
679 to Figure S1 (E).

680 **Figure S3. Active site conservation across evolution and alignment of SMG5. Related to**
681 **Figures 1, 2, S1 and S2.**
682 (**A**) Model of the complex between extended PIN domains of *Dm*Smg5 (purple, pink) and Smg6 (light
683 and dark green) based on the AlphaFold3 model of the full-length *Dm*Smg5-6 complex with U_6-RNA
684 and 2 Mg^{2+}. RNA (grey) and metal ions (yellow spheres) indicate the active site location, for which a
685 detailed view with active site residues shown as sticks and labelled is given below.
686 (**B**) Same as in (A) but for the model of the *Ce*SMG-5-6 PIN domain complex.
687 (**C**) Sequence alignment of the extended SMG5 PIN domain including α1 helix. Orthologs from *Homo*
688 *sapiens* (*Hs*), *Mus musculus* (*Mm*), *Gallus gallus* (*Gg*), *Xenopus tropicalis* (*Xt*), *Danio rerio* (*Dr*),
689 *Strongylocentrotus purpuratus* (*Sp*, Purple urchin), *Drosophila melanogaster* (*Dm*) and
690 *Caenorhabditis elegans* (*Ce*) are compared, and residues with complete conservation and 70%
691 similarity are highlighted in dark and light purple, respectively. Predicted secondary structure
692 elements of *Hs* and *Ce* proteins are denoted above and below the alignment, respectively. Residues
693 involved in the predicted SMG6 interface (green), active site metal coordination (yellow) and RNA
694 substrate binding (grey) are indicated by circles above the alignment. Red stars mark amino acids
695 that were mutated in this study.

696 **Figure S4. Extended mutational analysis confirms composite active site and PIN-PIN interface**
697 **in SMG5-SMG6 complex. Related to Figure 6.**
698 (**A**) As in main Figure 6C, analysis of kinetic differences between active site mutants (SMG5 D893A,
699 K896A, K897A and SMG6 D1353A), here in the SpyTag-SMG5 PIN(α-extension) / SpyCatcher-
700 SMG6 PIN(α-extension) setup.

701 (**B**) Observed rate constants (k_{obs}) calculated from each sample shown in (A). Data are plotted as
702 means ± SD. The *P*-values were calculated using two-tailed unpaired *t*-test.
703 (**C**) Related to main Figure 6E, this experiment shows the analysis of interaction surface mutant
704 SMG6 V1397E, using SMG5 PIN(α-extension) and SMG5 PIN(14-3-3-extension) setup.
705 (**D**) Observed rate constants (k_{obs}) calculated from data in (B). Data are plotted as means ± SD. The
706 *P*-values were calculated using two-tailed unpaired *t*-test.
707 (**E**) Similar experiment as in (C), probing the interaction surface mutant SMG6 V1397E, but in the
708 SpyTag-SMG5 PIN(α-extension) / SpyCatcher-SMG6 PIN(α-extension) setup.
709 (**F**) Observed rate constants (k_{obs}) calculated from data in (E). Data are plotted as means ± SD. The
710 *P*-values were calculated using two-tailed unpaired *t*-test.

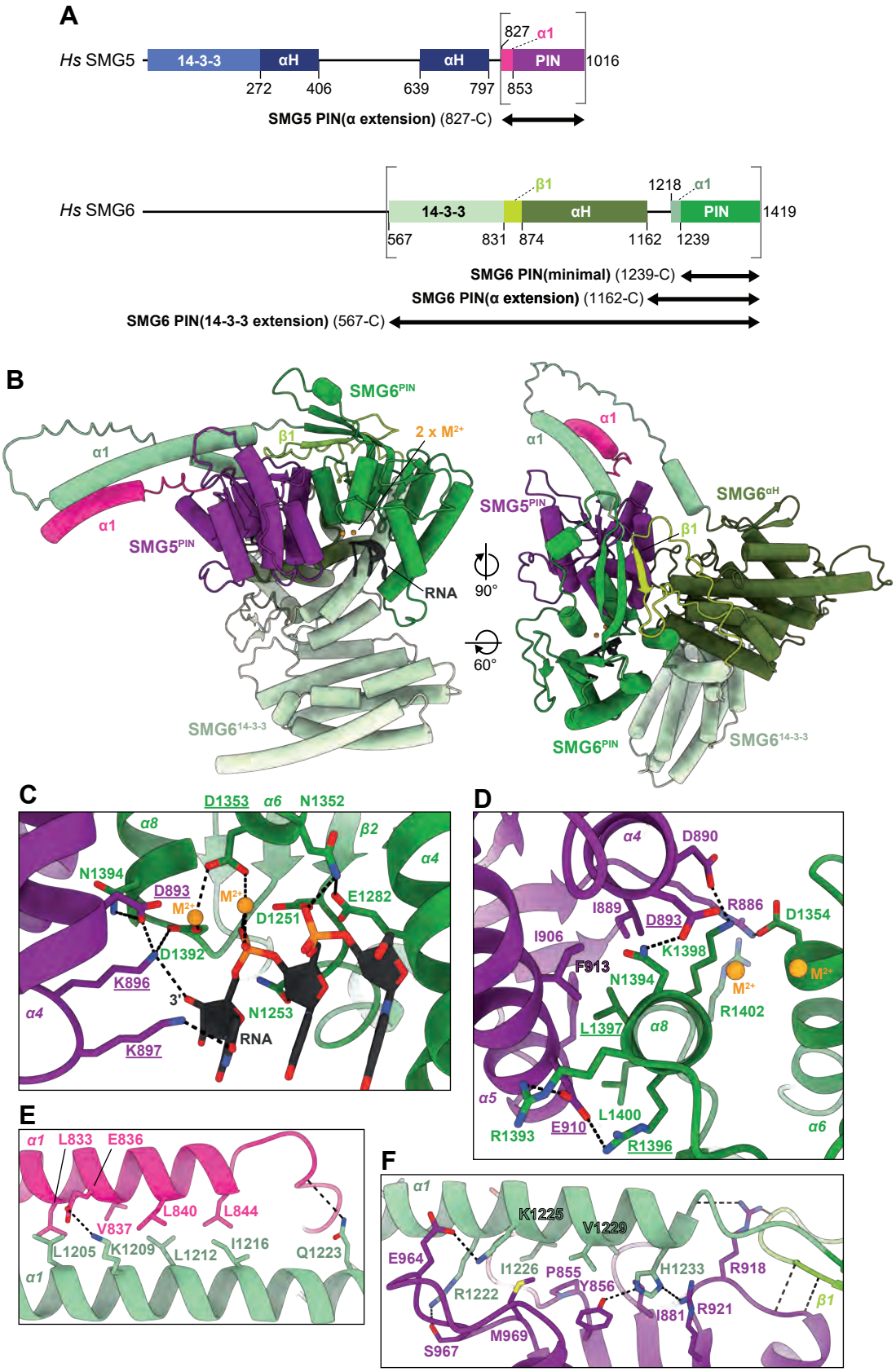
A
Hs SMG5
14-3-3
αH
αH
PIN
827
α1
1016
272
406
639
797
853
SMG5 PIN(α extension) (827-C)
Hs SMG6
14-3-3
β1
αH
1218
α1
PIN
1419
567
831
874
1162
1239
SMG6 PIN(minimal) (1239-C)
SMG6 PIN(α extension) (1162-C)
SMG6 PIN(14-3-3 extension) (567-C)
B
SMG6PIN
2 x M2+
α1
β1
α1
SMG5PIN
RNA
SMG6αH
90°
60°
SMG6PIN
SMG6 14-3-3
C
D1353
α6
N1352
α8
β2
α4
N1394
D893
M2+
E1282
D1251
D1392
K896
3'
N1253
RNA
K897
D
α4
D890
I889
R886
D1354
D893
I906
K1398
F913
N1394
M2+
R1402
L1397
α8
α5
L1400
R1393
E910
R1396
α6
E
α1
L833
E836
L840
L844
V837
L1205
K1209
L1212
I1216
Q1223
F
α1
K1225
V1229
E964
I1226
P855
H1233
R918
R1222
Y856
I881
R921
β1
M969
S967

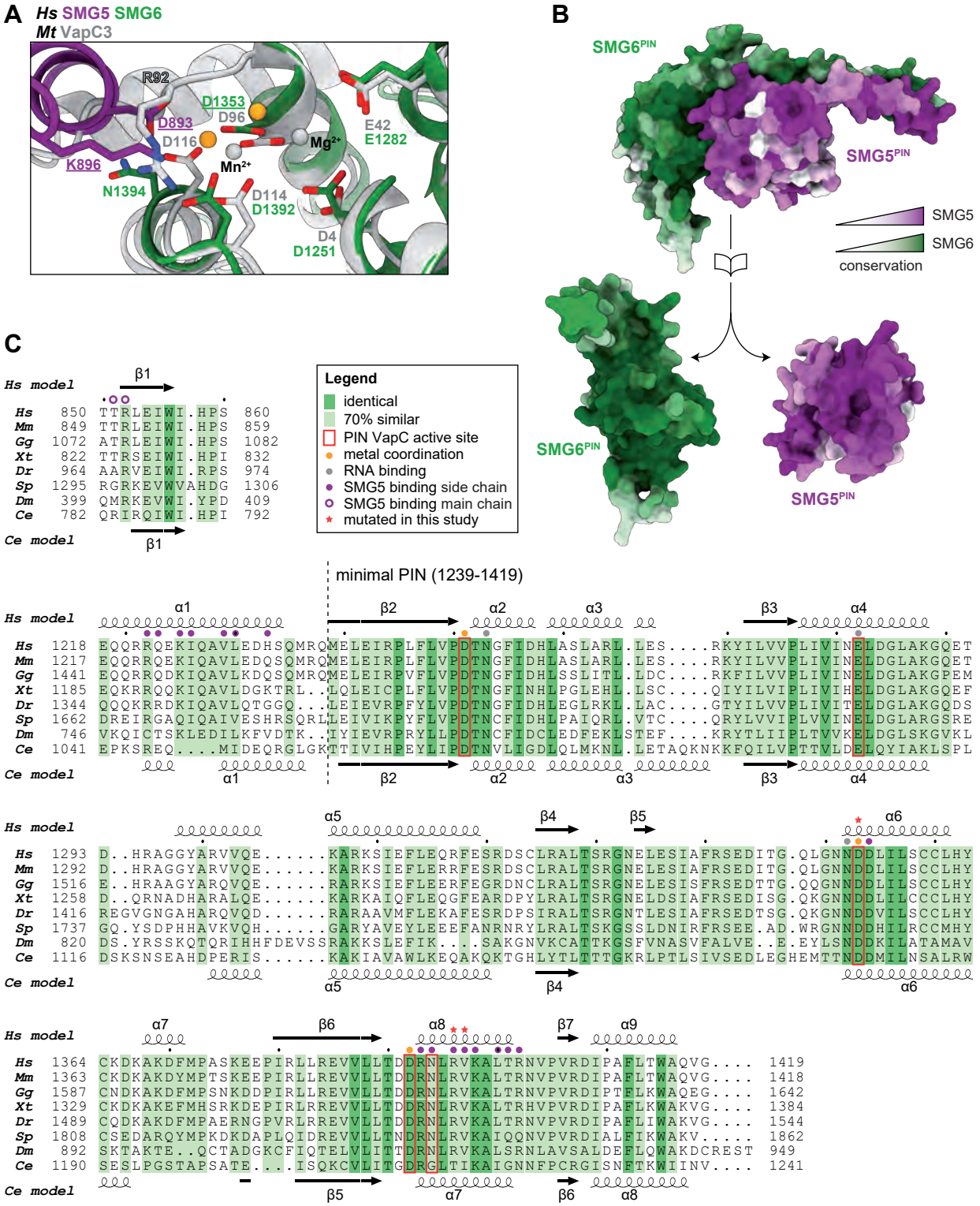
A
Hs SMG5 SMG6
Mt VapC3
R92
D1353
D96
D893
D116
Mg2+
E42
E1282
K896
Mn2+
N1394
D114
D1392
D4
D1251
B
SMG6PIN
SMG5PIN
SMG5
SMG6
conservation
SMG6PIN
SMG5PIN
C
Hs model
β1
Hs 850 TTRLEIWI.HPS 860
Mm 849 TTRLEIWI.HPS 859
Gg 1072 ATRLEIWI.HPS 1082
Xt 822 TTRSEIWI.HPI 832
Dr 964 AARVEIWI.RPS 974
Sp 1295 RGRKEVWVAHDG 1306
Dm 399 QMRKEVWI.YPD 409
Ce 782 QRIRQIWI.HPI 792
Ce model
β1
Legend
identical
70% similar
PIN VapC active site
metal coordination
RNA binding
SMG5 binding side chain
SMG5 binding main chain
mutated in this study
minimal PIN (1239-1419)
Hs model
α1 β2 α2 α3 β3 α4
Hs 1218 EQQRRQEKIQAVLEDHSQMRQMELEIRPLFLVPDTNGFIDHLASLARL.LES....RKYILVVPLIVINELDGLAKGQET
Mm 1217 EQQRRQEKIQAVLEDQSQMRQMELEIRPLFLVPDTNGFIDHLASLARL.LES....RKYILVVPLIVINELDGLAKGQET
Gg 1441 EQQRRQDKIQAVLKDQSQMRQMELEIRPVFLVPDTNGFIDHLSSLITL.LDC....RKFILVVPLIVINELDGLAKGPEM
Xt 1185 EQKRRQQKIQAVLDGKTRL..LQLEICPLFLVPDTNGFINHLPGLEHL.LSC....QIYILVIPLIVIHELDGLAKGQEF
Dr 1344 QQQKRRDKIQAVLQTGGQ...LEIEVRPFYLVPDTNGFIDHLEGLRKL.LAC....GTYILVVPLIVITELDGLAKGQDS
Sp 1662 DREIRGAQIQAIVESHRSQRLLEIVIKPYFLVPDTNCFIDHLPAIQRL.VTC....QRYLVVIPLVVINELDGLARGSRE
Dm 746 VKQICTSKLEDILKFVDTK..IYIEVRPRYLLPDTNCFIDCLEDFEKLSTEF....KRYTLIIPLTVVKELDGLSKGVKL
Ce 1041 EPKSREQ....MIDEQRGLGKTTIVIHPEYLIPDTNVLIGDLQLMKNL.LETAQKNKKFQILVPTTVLDELQYIAKLSPL
Ce model
α1 α2 α3 β3 α4
Hs model
α5 β4 β5 α6
Hs 1293 D..HRAGGYARVVQE.....KARKSIEFLEQRFESRDSCLRALTSRGNELESIAFRSEDITG.QLGNNDDLILSCCLHY
Mm 1292 D..HRAGGYARVVQE.....KARKSIEFLERRFESRDSCLRALTSRGNELESIAFRSEDITG.QLGNNDDLILSCCLHY
Gg 1516 E..HRAAGYARQVQE.....RARKSIEFLEERFEGRDNCLRALTSRGNELESISFRSEDTTG.QQGNNDDLILSCCLHY
Xt 1258 D..QRNADHARALQE.....KARKAIQFLEQGFEARDPYLRALTSRGNELDSIAFRSEDISG.QKGNNDDLILCCCLHY
Dr 1416 REGVGNGAHARQVQD.....RARAAVMFLEKAFESRDPSIRALTSRGNTLESIAFRSEDTSG.QKGNNDDVILSCCLHY
Sp 1737 GQ.YSDPHHAVKVQH.....GARYAVEYLEEEFANRNRYLRALTSKGSSLDNIRFRSEE.AD.WRGNNDDHILRCCMHY
Dm 820 DS.YRSSKQTQRIHHFDEVSSRAKKSLEFIK....SAKGNVKCATTKGSFVNASVFALVE..E.EYLSNDDKILATAMAV
Ce 1116 DSKSNSEAHDPERIS.....KAKIAVAWLKEQAKQKTGHLYTLTTTGKRLPTLSIVSEDLEGHEMTTNDDMILNSALRW
Ce model
α5 β4 α6
Hs model
α7 β6 α8 β7 α9
Hs 1364 CKDKAKDFMPASKEEPIRLLREVVLLTDDRNLRVKALTRNVPVRDIPAFLTWAQVG.... 1419
Mm 1363 CKDKAKDYMPTSKEEPIRLLREVVLLTDDRNLRVKALTRNVPVRDIPAFLTWAQVG.... 1418
Gg 1587 CNDKAKDFMPSNKDDPIRLLREVVLLTDDRNLRVKALTRNVPVRDIPTFLKWAQEG.... 1642
Xt 1329 CKDKAKEFMHSRKDEPIRLRREVVLLTDDRNLRVKALTRHVPVRDIPAFLKWAKVG.... 1384
Dr 1489 CQDKAKDFMPAERNGPVRLRREVVLLTDDRNLRVKALTRNVPVRDIPAFLIWAKVG.... 1544
Sp 1808 CSEDARQYMPKDKDAPLQIDREVVLLTNDRNLRVKAIQQNVPVRDIALFIKWAKV..... 1862
Dm 892 SKTAKTE..QCTADGKCFIQTELVLITTDRNLRVKALSRNLAVSALDEFLQWAKDCREST 949
Ce 1190 SESLPGSTAPSATE....ISQKCVLITGDRGLTIKAIGNNFPCRGISNFTKWIINV.... 1241
Ce model
β5 α7 β6 α8

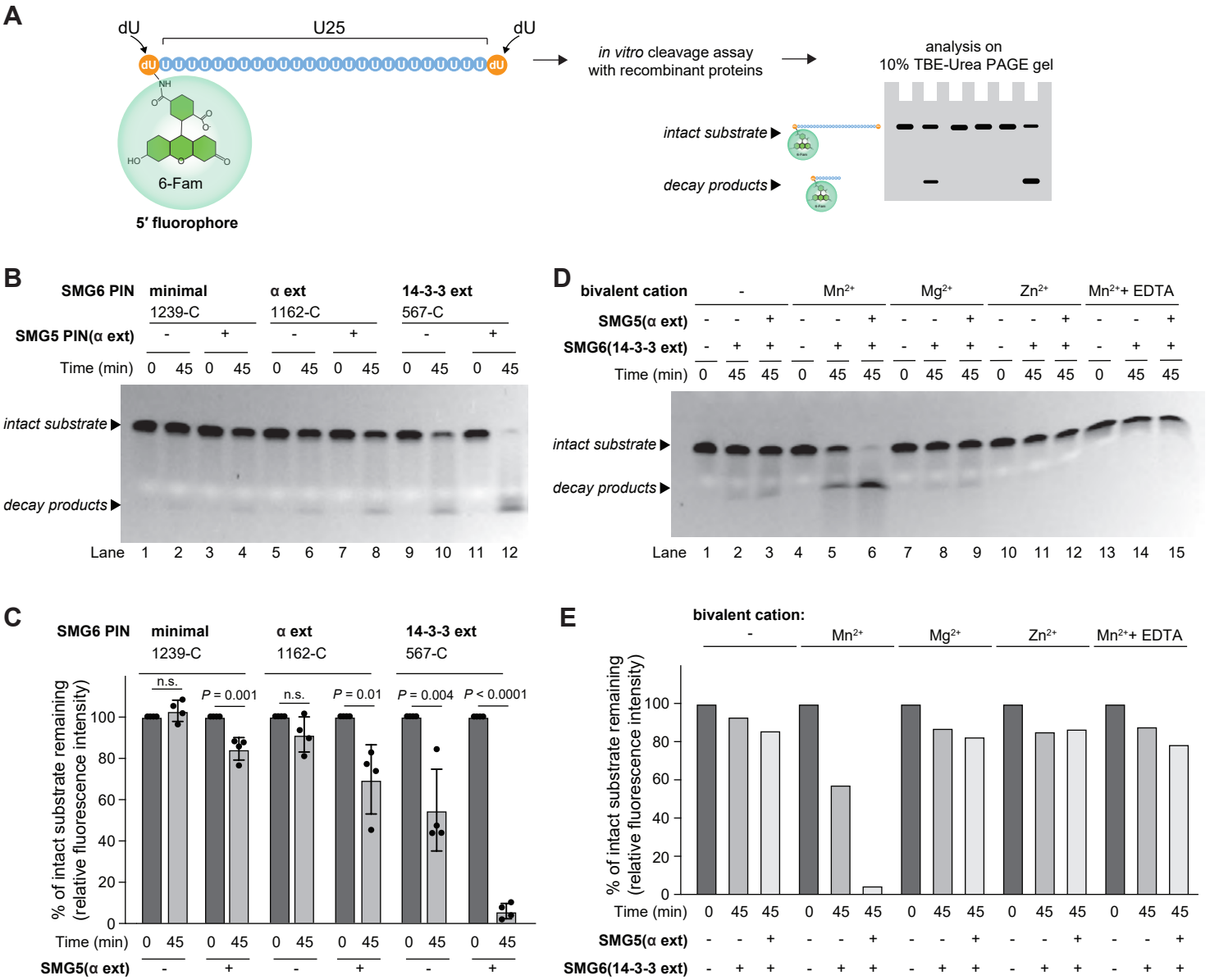
A
dU
U25
dU
6-Fam
5′ fluorophore
in vitro cleavage assay
with recombinant proteins
analysis on
10% TBE-Urea PAGE gel
intact substrate
decay products
B
SMG6 PIN
minimal
1239-C
α ext
1162-C
14-3-3 ext
567-C
SMG5 PIN(α ext)
Time (min)
intact substrate
decay products
Lane
D
bivalent cation
Mn2+
Mg2+
Zn2+
Mn2+ + EDTA
SMG5(α ext)
SMG6(14-3-3 ext)
Time (min)
intact substrate
decay products
Lane
C
SMG6 PIN
minimal
1239-C
α ext
1162-C
14-3-3 ext
567-C
n.s.
P = 0.001
n.s.
P = 0.01
P = 0.004
P < 0.0001
% of intact substrate remaining
(relative fluorescence intensity)
Time (min)
SMG5(α ext)
E
bivalent cation:
Mn2+
Mg2+
Zn2+
Mn2+ + EDTA
% of intact substrate remaining
(relative fluorescence intensity)
Time (min)
SMG5(α ext)
SMG6(14-3-3 ext)

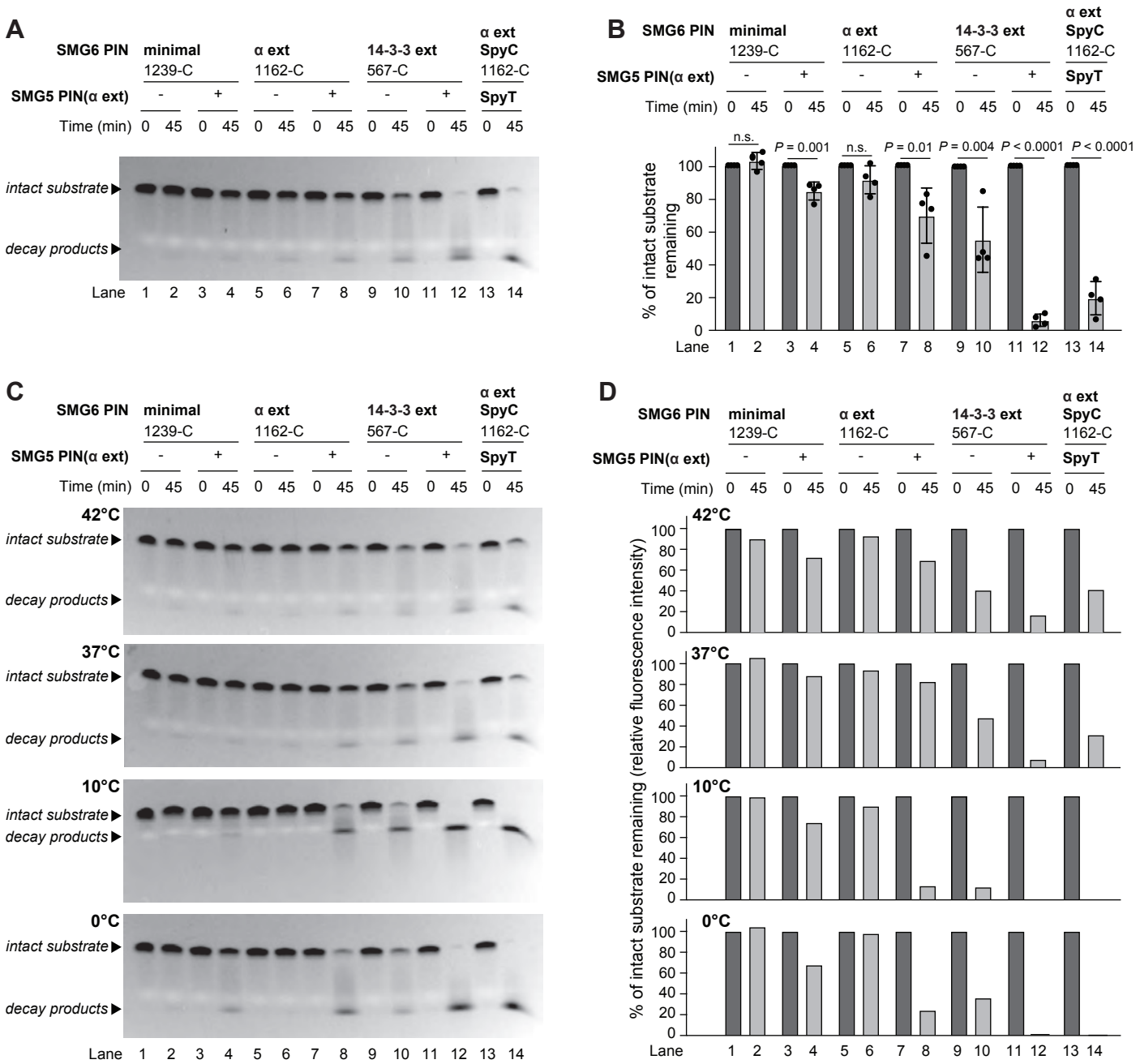
A
SMG6 PIN
minimal
1239-C
α ext
1162-C
14-3-3 ext
567-C
α ext
SpyC
1162-C
SMG5 PIN(α ext)
-
+
SpyT
Time (min)
0 45
intact substrate
decay products
Lane 1 2 3 4 5 6 7 8 9 10 11 12 13 14
B
% of intact substrate remaining
n.s.
P = 0.001
P = 0.01
P = 0.004
P < 0.0001
P < 0.0001
C
42°C
37°C
10°C
0°C
D
% of intact substrate remaining (relative fluorescence intensity)

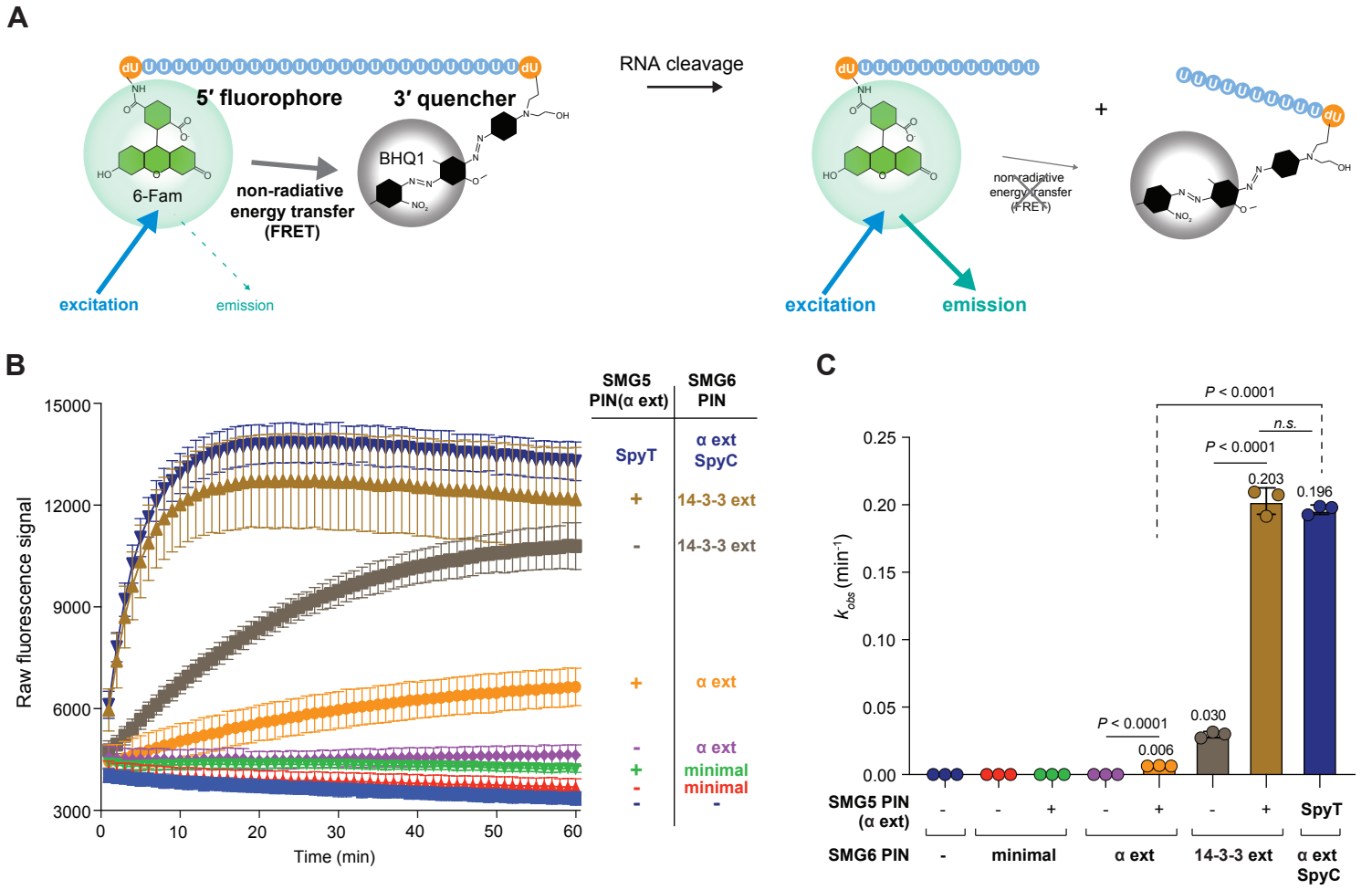
A
5′ fluorophore
3′ quencher
6-Fam
BHQ1
non-radiative energy transfer (FRET)
excitation
emission
RNA cleavage
B
Raw fluorescence signal
Time (min)
SMG5 PIN(α ext)
SMG6 PIN
SpyT
α ext SpyC
+
14-3-3 ext
-
14-3-3 ext
+
α ext
-
α ext
+
minimal
-
minimal
-
-
C
k_{obs} (min^{-1})
P < 0.0001
n.s.
P < 0.0001
0.203
0.196
P < 0.0001
0.030
0.006
SMG5 PIN (α ext)
SMG6 PIN
minimal
α ext
14-3-3 ext
α ext SpyC
SpyT

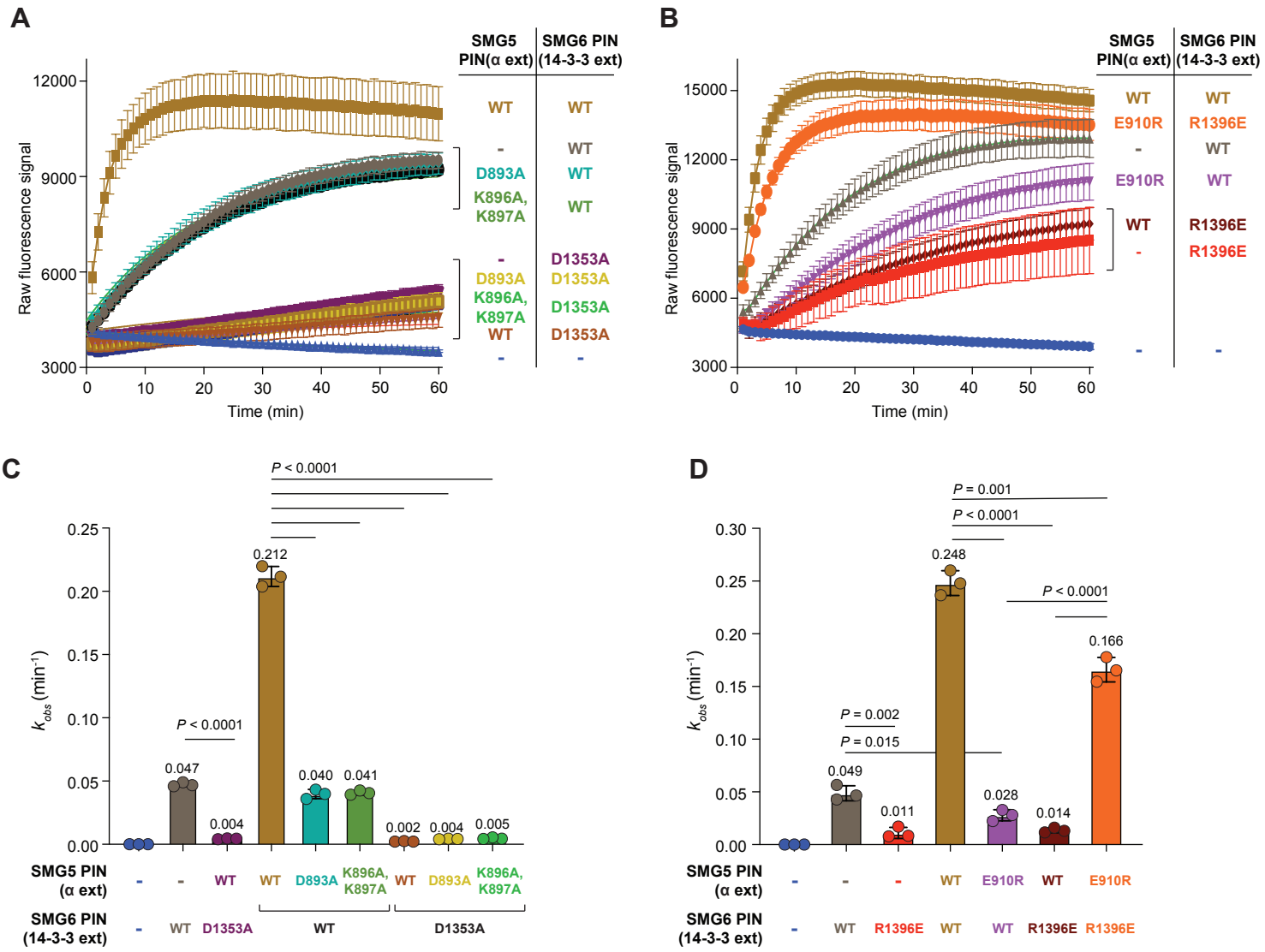
A
SMG5 PIN(α ext)
SMG6 PIN (14-3-3 ext)
Raw fluorescence signal
Time (min)
WT WT
- WT
D893A WT
K896A, K897A WT
- D1353A
D893A D1353A
K896A, K897A D1353A
WT D1353A
- -
B
SMG5 PIN(α ext)
SMG6 PIN (14-3-3 ext)
Raw fluorescence signal
Time (min)
WT WT
E910R R1396E
- WT
E910R WT
WT R1396E
- R1396E
- -
C
P < 0.0001
P < 0.0001
k_{obs} (min^{-1})
0.047
0.004
0.212
0.040
0.041
0.002
0.004
0.005
SMG5 PIN (α ext)
SMG6 PIN (14-3-3 ext)
D
P = 0.001
P < 0.0001
P = 0.002
P = 0.015
P < 0.0001
k_{obs} (min^{-1})
0.049
0.011
0.248
0.028
0.014
0.166
SMG5 PIN (α ext)
SMG6 PIN (14-3-3 ext)